This is a repository copy of *Inhibition of ATR opposes glioblastoma invasion through disruption of cytoskeletal networks and integrin internalisation via macropinocytosis*.

White Rose Research Online URL for this paper:
https://eprints.whiterose.ac.uk/205237/

Version: Published Version

Article:

Inhibition of ATR opposes glioblastoma invasion through disruption of cytoskeletal networks and integrin internalisation via macropinocytosis

Derby S[1†], Dutton L[1†], Strathdee KE[1], Stevenson K[1], Koessinger A[1,2], Jackson M[1], Yuling Tian[1], Wenxi Yu[1], Mclay K[1], Misquitta J[1], Alsharif S[1] , Clarke CJ[2], Gilmour L[1], Thomason P[2], McGhee E[2], McGarrity-Cottrell CL[3], Vanderlinden A[3], Collis SJ[3], Rominyi O[3], Lemgruber L[4], Solecki G[5], Olson M[8], Winkler F[6], Carlin LM[1,2], Heiland DH[7], Inman G[1,2], Chalmers AJ[1], Norman JC[1,2] ,Carruthers R[1] and Birch JL[1*]

[1] Wolfson Wohl Translational Cancer Research Centre, School of Cancer Sciences, University of Glasgow, UK

[2]CRUK Scotland Institute , Glasgow, UK

[3]Department of Oncology and Metabolism, The University of Sheffield Medical School, Sheffield, UK

[4]Cellular Analysis Facility, College of Medical, Veterinary & Life Sciences, University of Glasgow, UK

[5] Business Unit Service and Customer Care, Carl Zeiss Microscopy GmbH, 07745 Jena, German

[6] German Cancer Consortium (DKTK), German Cancer   Research Center (DKFZ), Heidelberg

[7] MILO Laboratory, Department of Neurosurgery, Freiburg, Germany

[8] Ryeson University, Toronto, Canada

*Address for correspondence. Dr Joanna Birch, Wolfson Wohl Translational Cancer Research Centre, School of Cancer Sciences, University of Glasgow, UK. Email Joanna.birch@glasgow.ac.uk.

†Authors have made an equal contribution and the order of names is interchangeable

Conflict of interest: None declared.

Data Availability: Data will be made available upon reasonable request.

Abstract

Background

Glioblastomas have highly infiltrative growth patterns that contribute to recurrence and poor survival. Despite infiltration being a critical therapeutic target, no clinically useful therapies exist which counter glioblastoma invasion. Here, we report that inhibition of Ataxia telangiectasia and Rad 3 related kinase (ATR) reduces invasion of glioblastoma cells through dysregulation of cytoskeletal networks and subsequent integrin trafficking.

Methods

Glioblastoma motility and invasion were assessed *in vitro* and *in vivo* in response to ATR inhibition (ATRi) and ATR over-expression using timelapse microscopy, two orthotopic glioblastoma models and intravital imaging. Disruption to cytoskeleton networks and endocytic processing were investigated via high throughput, super resolution imaging and intravital imaging.

Results

High ATR expression was associated with significantly poorer survival in clinical datasets whilst histological, protein expression and spatial transcriptomics using glioblastoma tumour specimens revealed higher ATR expression at infiltrative margins. Pharmacological inhibition with two different compounds and RNAi targeting of ATR opposed invasion of glioblastoma, whereas overexpression of ATR drove migration. Subsequent investigation revealed that cytoskeletal dysregulation reduced macropinocytotic internalisation of integrins at growth cone-like structures, resulting in a tumour microtube retraction defect. The biological relevance and translational potential of these findings was confirmed using two orthotopic *in vivo* models of glioblastoma and intravital imaging.
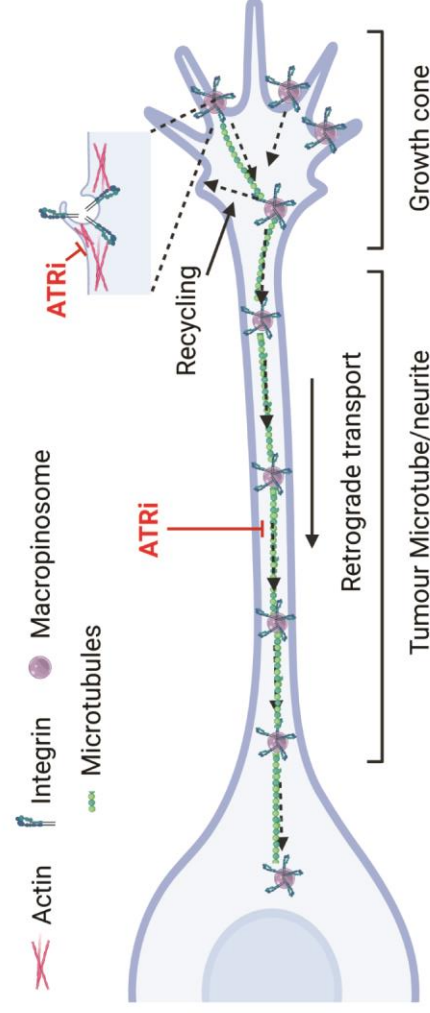
Conclusion

We demonstrate a novel role for ATR in determining invasion in glioblastoma cells and propose that pharmacological targeting of ATR could have far reaching clinical benefits beyond radiosensitisation.

2

Graphical abstract

Key points (3)

1) ATR expression is elevated in tumour margin regions of human glioblastoma samples and is associated with poorer survival.
2) ATR promotes glioblastoma cell invasion via the internalisation and trafficking of integrins.
3) Pharmacological inhibition of ATR reduces glioblastoma invasion.

Importance of the study

Invasion of vital neural structures is the cause of distressing morbidity and a contributing cause of death in glioblastoma patients. Despite infiltration being an obvious therapeutic target there are no anti-invasive agents currently in clinical use. ATR is a key DNA damage response protein involved in DNA replication stress and is the focus of intense interest as a potential radiosensitiser in other tumour types. We demonstrate a novel role for ATR in driving glioblastoma cell invasion and propose that ATR inhibitors will have beneficial therapeutic effects in this disease beyond radiation induced DNA damage potentiation.

4

Introduction

Glioblastoma is a treatment-refractory brain tumour with a profoundly invasive phenotype that prevents curative tumour resection. Brainstem invasion by glioblastoma cells is a common feature at autopsy, suggesting that infiltration not only contributes to neurological dysfunction, but also impacts on clinical outcome [1]. Median survival of patients undergoing maximal neurosurgical resection followed by adjuvant radiotherapy and chemotherapy is only 12 – 18 months [2]. Attempts to eradicate invasive microscopic disease by increasing the irradiated volume of brain have failed to improve survival and caused unacceptable toxicity [3,4]. More detailed understanding of the mechanisms involved in glioblastoma invasion has potential to reveal novel anti-invasive therapies that may enhance the efficacy of existing treatment regimens. Indeed several pre-clinical studies have indicated the value of this approach, but so far none has successfully translated into the clinic [5] [6] [7].

Ataxia telangiectasia and Rad 3 related (ATR) is a phosphatidylinositol 3-kinase (PI3K)-like kinase which is central to the DNA damage and replicative stress response in S phase of the cell cycle where it recruits DNA repair machinery and induces S phase arrest [8] [9] [10] [11]. These processes require regulation of nucleoskeletal components to maintain architecture during lesion resolution and to communicate induction of cell cycle arrest to the cytoskeleton [12], [13].

A non-canonical, cytoplasmic role for ATR has also emerged in recent years. Cara *et al* showed that the SCD protein domain targeted by ATR is commonly found in proteins involved in the nervous system, including proteins that regulate vesicle trafficking and cytoskeleton dynamics [14]. Additionally, several studies implicate ATR in cytoplasmic processes including the maintenance of nuclear plasticity [15], and facilitation of endocytosis and excitatory vesicle recycling at neuronal synapses [16]. The latter observation is of particular interest in glioblastoma cells which share a neural crest lineage and morphological features with neuronal cells, including structures that resemble axonal growth cones at the ends of neurite-like projections called tumour microtubes (TMs) [17]. TMs allow interconnectivity between glioblastoma cells and surrounding neuronal cells, forming a functional network that promotes treatment resistance and tumour cell infiltration [18] [19].

Macropinocytosis is an endocytic process facilitating cellular uptake of high molecular weight, extracellular material and is involved in nutrient uptake, antigen presentation and chemotactic responses [20] [21]. Effective macropinocytosis and trafficking of resultant endosomes requires coordinated activity of

5

the actin and microtubule components of the cytoskeleton [22]. Intriguingly, macropinocytosis at neuronal axonal growth cones determines repulsive axonal turning and retraction [23] [24]. Furthermore, macropinocytosis is implicated in the rapid trafficking of integrins from focal adhesions to cellular ventral surfaces during growth factor-stimulated cell motility [25] and in facilitating membrane recycling in neural crest cells to drive migration [26]. Dysregulated macropinocytosis has been documented in glioblastoma, but to date, a potential link between macropinocytosis and glioblastoma invasion is yet to be investigated [27,28].

Using *in vitro* and *in vivo* studies and four different primary glioblastoma lines we report a novel role for ATR in driving invasion of glioblastoma cells via the regulation of actin and microtubule networks that support turnover of integrins at growth cone-like structures. We demonstrate that this function of ATR is highly sensitive to pharmacological inhibition, resulting in abrogation of glioblastoma invasion both *in vitro* and *in vivo* and presents a novel clinical approach to disease management.

Methods

Derivation and maintenance of primary glioblastoma cell lines

Primary glioblastoma cell lines E2, G7, and R15 were derived from resected tumors (see supplementary methods) and maintained as neurospheres as described previously in stem cell enriched culture conditions [29] [30]. Cell lines were discarded after 10 passages and were tested for the presence of mycoplasma every 3 months and subjected to STR profiling to confirm authenticity. To provide adherent cells for experiments, stem-cell enriched neurosphere cultures of G7, E2, R15 and Ox5 were plated on Matrigel-coated plates (0.23 mg/L in AdDMEM, Life Technologies) in stem cell enriching media. S24-GFP cells were cultured as neurospheres as previously described [18].

In vitro irradiation was performed using an Xstrahl RX225 radiation cabinet (195 kV X-rays, dose rate 1.39 Gy/minute).

Integrin Internalisation assays

The assays used to measure integrin internalisation have previously been described [31]. Briefly, cells were labelled with NHS-SS-biotin and internalisation was allowed to continue at 37°C. Cells were then washed and lysed and levels of biotinylated integrin determined by capture-ELISA.

6

Cell viability

Cell viability was carried out using CellTiter-Glo according to the manufacturer's protocol (Promega). Briefly, cells were plated in Matrigel coated 96-well plates and incubated with incremental concentrations of drugs. Cells were irradiated with 2Gy one hour after addition of drug and incubated for a further 23 hours prior to detection of luminescence (Promega GLOMAX).

Spatial Transcriptomics

We obtained 16 de-novo glioblastoma samples from the Freiburg Spatial Transcriptomics database. The samples were prepared following the protocol outlined in the original publication (Ravi et al., 2022). We visualized gene expression levels using the SPATA2 package (Kueckelhaus et al., 2021) in R software. The SPATA2: plotSurface function was used to create 2D plots of gene expression across the tissue section. The color_by and alpha_by parameter was set to the gene expression levels. The display_image parameter was set to TRUE, which generated a visualization of the tissue section overlaid with the gene expression plot. We also applied the smooth function with the standard span-factor to generate a smoother representation of the gene expression data. We performed correlation analysis using the SPATAWrappers package (Ravi et al., 2022). The runSpatialRegression function was applied with a spatial lag model to identify pairwise correlations between gene expression levels and the abundance of gene signatures across the tissue section. The results of the correlation analysis were visualized using the corplot function, which generated a heatmap of the pairwise correlation coefficients.

siRNA and plasmid transfection

Subconfluent G7 cells were transfected with 30 pmol siRNA targeting ATR or control (Dharmacon: cat no J-003202-19-002 Lot no: 190724) using RNAiMAX reagent (Invitrogen 13778-030) and plated into 6 well plate then incubated for 48 hours prior to imaging or protein extractions. For ATR over-expression, G7 cells were transfected with either pcDNA3 or pcDNA3.ATR using SuperFect transcription reagent (Qiagen).

Sub confluent migration assays

Sub confluent migration assays were performed as previously described [5].

7

Immunofluorescence

For confocal imaging sub-confluent glioblastoma cells were plated on coverslips coated with Matrigel and incubated at 37°C for 24 hours. For high-throughput imaging, 1×10^4 cells were plated on 96 well black sided plates (Perkin Elmer) precoated with Matrigel. Cells were incubated with anti-ATR (23HCLC ThermoFisher) or anti-integrin a6 (CD49F 55734 BD Bioscience) antibodies overnight at 4°C followed by incubation with secondary conjugated antibodies, DAPI and HCS Cell Mask Deep Red Stain (ThermoFisher H32721) or Texas red-X Phalloidin (ThermoFisher T7471).

Confocal and High-throughput imaging

Images were acquired using either a Zeiss LSM 780 or 880 confocal microscope and analysed using Zen 2012 (Zeiss) or Imaris. For High-throughput analysis, images were captured using the Opera Phoenix High-content Screening system and analysed using Columbus Image Analysis software (Perkin Elmer).

Super resolution microscopy

For macropinocytosis capture, 0.5×10^5 G7 cells were plated on glass bottomed 35 mm dishes pre-coated with 5μg/ml fibronectin (ThermoFisher) and allowed to establish for 24 hours. 1μg of plasmid containing α5-GFP was then transiently transfected into cells using SuperFect transcription reagent (Qiagen). After 24 hours, 0.1 mg/ml lysine fixable, 70kDa Texas-red dextran was added, and cells allowed to internalise for 30 mins before addition of either DMSO or VE822. For tracking of macropinocytosis, timelapse, super resolution imaging was performed using Zeiss 880 Airyscan (SR mode) with a Plan-Apochromat 40x/1.3 Oil objective and images analysed using Imaris software. Cell were maintained at 37°C, 5% CO2 in an incubation chamber for the duration of imaging.

For EB1 tracking, G7 cells were transfected with pEGFP-EB1 (kindly provided by Prof. Laura Machesky, Cambridge) followed by treatment with DMSO, 1μM VE822, or 1μM Bayer 1895344 for 16 hours before imaging. Images of EB1-GFP were acquired on a Zeiss Elyra 7 microscope using a 40x NA1.2 water immersion objective and full environmental control to deliver 37C and 5% CO2. 5-phase apotome with z-leap mode was used (0.373um spacing). Images were captured onto a pcoEDGE 4.2M sCMOS camera using a 50ms exposure time. Frame interval between captures was 2 sec. Raw images were SIM-processed using the "standard" setting in Zen black software.

8

Animal experiments

Animal experiments were performed under the relevant home office licence and in accordance with ARRIVE guidelines. All experiments had ethical approval from the University of Glasgow under the Animal (Scientific Procedures) Act 1986 and the EU directive 2010. Mice were maintained in individually ventilated cages with environmental enrichment.

Intracranial window experiments

Male NMRI-*Foxn1^nu* mice (n=5) were used for this experiment using a previously described protocol [32]. 2-3 weeks after window implantation, mice were injected with 30,000 S24-GFP cells and tumours allowed to develop for a further 2-3 weeks.

Mice were given either vehicle (10% vitamin E) or VX970 (50mg/kg) by oral gavage according to the schedules described in the results section. 200μl of 10mg/ml 10kDa dextran was administered subcutaneously. 10kDa dextran was used to allow multiple subcutaneous injections efficient delivery across the blood-brain barrier. 10kDa dextran can be internalised by other endocytic processes, however a significant amount is internalised via macropinocytosis [33]. *In vitro* uptake assays confirmed that its endocytosis was similarly impacted by ATR inhibition (data not shown). For imaging details, see supplemental M&M.

Multi photon *intravital* imaging

Imaging was undertaken using a Zeiss LSM880 NLO multiphoton microscope using W Plan-Apochromat 20x/1.0 NA water immersion objective and subsequently analysed using Imaris software. Z-stacks were taken to a depth of 60 – 100 μm, at 1μm intervals. GFP and TR-dex were excited using a Coherent Discovery '2-photon' laser tuned to 890nm, CB dex tuned to 800nm. Signals were acquired onto GaAsP non-descanned detectors.

Intracranial tumour experiments

Female CD1 nude mice were orthotopically injected with 1×10^5 G7 or S24-GFP cells as previously described [5] before dosing with either vehicle (10% vitamin E) or 60mg/kg VX970 and mice culled at the indicated time points. For PK analysis, tumors were sub-dissected and fresh-frozen specimens of blood, tumour and contralateral hemispheres sent for PK analysis (Vertex). For the invasion study, tumours were allowed to establish for 2 weeks (S24) or 10 weeks (G7) mice before daily dosing for 10 days with either vehicle (10% vitamin E) or 50mg/kg VX970. Formalin-fixed, paraffin-embedded sections were stained for

9

Ki67, and scanned using a Hamamatsu Nanozoomer Slide scanning machine and automated analysis conducted using QuPath software.

Results

ATR is found in the cytoplasm of glioblastoma cells, and its expression correlates with invasive potential.

Nuclear ATR activation in response to replication stress has previously been described as a hallmark of glioblastoma cells [9]. Consistent with previous reports in other cell types, confocal immunofluorescence imaging of glioblastoma cells also showed ATR to also be present in the cytoplasm of primary glioblastoma cell lines (Fig 1A (i), (ii)).)). Cytoplasmic localisation was confirmed with a second antibody (Fig S1A), and via subcellular fractionation of lysates from three primary glioblastoma lines (Fig S1B). Furthermore, high-throughput imaging and automated quantification of cells subjected to a sublethal dose of radiation (RT; 2Gy), which is known to induce motility in glioblastoma cells [5-7], revealed a significant increase in cytoplasmic ATR (fig 1B (i), (ii), Fig S1B).

Interrogation of two publicly available datasets of mRNA expression in glioma (TCGA and CGCA) showed that ATR expression increased with tumour grade, being elevated in highly infiltrative Grade IV tumours compared with lower grade gliomas (Fig 1C (i); Fig S1C). Higher ATR expression also correlated with poorer survival in three separate datasets (Fig 1C (ii), (iii); Fig S1D). Although the reasons behind these observations are likely manifold, the contribution of infiltration to patient survival [1] indicates an intriguing link between ATR and tumour invasion.

In three human glioblastoma specimens, immunohistochemical studies identified increased pATR expression at the invading edge in matched tumour core and margin samples (Fig 1D (i)). This observation was independently confirmed by western blot analysis of freshly cultured Ox5 primary glioblastoma cells isolated from core and margin tumour regions (Fig 1E (i), (ii)). Lastly, we examined the spatial expression profile of ATR utilizing the Freiburg spatial transcriptomic atlas, which comprises 16 de-novo glioblastoma specimens [34]. ATR expression was observed to be associated with histological regions, including pseudopalisading, perinecrotic areas, and microvascular proliferation, as classified by the Ivy glioblastoma atlas. These characteristic glioblastoma structures are linked to increased invasive capacity (Fig 1F (i)). To further investigate the spatial correlation between ATR gene expression and the abundance of known expression subgroups, we applied a spatial lag model for correlation analysis. ATR expression demonstrated variability across subtypes but exhibited increased levels in subtypes associated with enhanced migration/infiltration, such as injury response and Neftel MES 1 (Fig 1F (ii)) [35].

10

These results, from three independent data sets, indicate a potentially clinically relevant association between ATR expression and infiltration.

ATR is required to drive glioblastoma cell migration *in vitro.*

To investigate the functional role of cytoplasmic ATR, 3 primary glioblastoma lines (G7, E2 and R15) were treated with the ATR inhibitor, (VE822/VX970/Berzosertib), referred to as ATRi henceforth), followed by subconfluent migration assays (Fig 2A (i)-(iii)). ATRi significantly reduced migration speed of all three glioblastoma lines at concentrations > 10-fold below those required to impact on cell viability after 24 hours exposure (Fig. 2B (i), (ii); Fig S2A; Table S1). This data suggests that ATR has a specific role in regulating the invasive potential of glioblastoma cells that is independent of its role in DNA damage response. As radiotherapy (RT) is given as standard of care to all glioblastoma patients, and radiation has previously been reported to induce invasion of glioblastoma cells [5-7], we repeated the experiment following treatment of cells with 2Gy radiation. Interestingly, we observed an increased sensitisation of two out of three of the cell lines after radiation (Table S1).

VE822/VX970 is a well characterised and highly specific inhibitor of ATR, and its efficacy as an anti-invasive compound at low concentrations suggests that our observations reflect on-target effects of the inhibitor. However, to confirm this, we performed sub-confluent migration assays following exposure to both an additional ATR inhibitor, Bay1895344 (ATRiB) in all three lines (Fig 2C(i); Fig S2B), and siRNAs and CRISPR deletions targeting ATR in in the most genetically tractable glioblastoma line, G7 (Fig 2C (i), (ii); Fig S2C). The results demonstrated a significant decrease in migration speed under all conditions, providing confirmation of an on-target effect of ATR inhibition on motility. Western blots for pChk1 (a nuclear target of ATR) were conducted to ensure drug efficacy at the chosen concentration (Fig S2D). The motility data was further confirmed using a more complex 3D invasion assay using Matrigel coated scaffolds plated with E2 and R15 cells (Fig S2E (i), (ii))[36].

The above data strongly indicates that ATR is required to support glioblastoma cell migration *in vitro*. To ascertain whether ATR is also able to actively drive migration, we over-expressed ATR in G7 cells. We observed a significant increase in migration speed, indicating that ATR may indeed play an active role in migration induction (Fig 2D (i)-(iii)). Interestingly, preliminary data suggests that the role in invasion may be unique to ATR, since inhibiting two other DNA damage response factors (PARP and ATM) had no effect on migration in any of the three cell lines tested (Fig S2F).

11

Inhibition of ATR increases cytoplasmic macropinosomes.

In addition to migration defects, treatment with ATRi, ATRiB or siRNA mediated knockdown of ATR increased the appearance of enlarged vacuolar structures within the cytoplasm of glioblastoma cells (Fig 3A(i) and (ii); Fig S3A). We conducted a series of experiments to elucidate the origin of these structures. Autophagy has been demonstrated to modulate cell migration and integrin membrane recycling [37]. To investigate whether a dysregulation of autophagy was underpinning our observations, we undertook autophagic flux assays as previously described [38]. Western blot analysis for processed LC3B from cells treated with/without VE822 and chloroquine indicated no change in the levels of LC3B II, indicating that the observed vacuoles were unlikely to be derived from a block in autophagy (Fig S3B). Indeed, electron microscopy revealed the vacuoles to be single membrane bound, inconsistent with autophagosomes (Fig 3B). This data demonstrates that autophagy likely does not contribute to the observed phenotype.

Next, we investigated whether these structures could be macropinosomes, which are characteristically large (0.2 - 5µm) and bound by a single membrane. G7 cells were incubated with a Texas red labelled 70kDa dextran (red) in the presence of ATRi. Dextrans of this size are predominantly internalised via macropinocytosis, and is an established method to mark cellular structures that result from this endocytic process [39]. The cells were fixed, stained and subjected to confocal imaging (Fig 3C (i), (ii)). Indeed, a large proportion of the vacuoles contained dextran, identifying them as macropinosomal in origin. Localisation was confirmed as intracellular via z-stack reconstruction (Fig S3 C).

To confirm biological relevance, we used orthotopic *intravital* imaging to look for dextran accumulation in GFP-S24 cells *in vivo* (Fig 3D (i)). Using advanced imaging and processing with Imaris software we were able to confidently detect internalised fluorescent dextran within GFP-S24 cells within the mouse brain (Fig 3D (ii)). The longitudinal nature of this technique, allows each mouse to be used as its own control. Mice (n=5) were initially treated on two consecutive days with vehicle alongside cascade blue-dextran (CB-dex), before multiphoton imaging. They were then treated twice with ATRi alongside Texas red-dextran (TR-dex), before repeat imaging (Fig 3C (iii)). By changing the colour of the dextran label, we ensured that only dextran internalisation/processing that may have been affected by ATRi treatment was detected in the second imaging session. To control for any variance in fluorophore detection affecting results, the order of administration of dextran colours was switched in one mouse (TR-dex/veh then CB-dex/ATRi), and an additional mouse was treated with ATRi and CB-dex alone. Subsequent colocalization analysis revealed that ATRi caused an accumulation of dextran in GFP-S24 cells, confirming the biological relevance of our *in vitro* findings (Fig 3D (iv)).

12

ATRi causes a block in both active macropinocytosis and processing of internalised macropinosomes.

To test whether the increase in macropinosomes was due to an increase in active macropinocytosis or a block in processing of internalised macropinosomes we conducted a pair of timed experiments. Firstly, cells were treated with either DMSO, ATRi or an inhibitor of macropinocytosis (EIPA, positive control) for 15mins or 2 hours prior to the addition of 70kDa Fluorescein-dex. Cells were allowed to internalise dextran for 30 mins before fixing (at 15 or 120mins), staining and high-throughput imaging and automated analysis (Fig 3E (i)). We observed a significant dose-dependent decrease in dextran positive macropinosomes in ATRi and ATRiB pre-treated cells using all three cell lines (Fig 3E (ii); Fig S3D (i),(ii)), indicating a block in active macropinocytosis.

With inhibition of active macropinocytosis being observed upon pre-treatment with ATRi (Fig 3E (ii)), but a clear accumulation of dextran positive macropinosomes apparent when ATRi and dextran are given concomitantly (Fig 3C), we concluded that a block in the lysosomal processing of cytoplasmic macropinosomes, and thus degradation of dextran, must also be occurring. To confirm this, cells were allowed to internalise dextran for 30 mins in the absence of compound, prior to its removal and addition of DMSO, ATRi or EIPA for 15 mins (Fig 3A(ii)). Analysis showed turnover of pre-internalised dextran is reduced in a dose dependent manner in cells treated with ATRi, strongly suggesting that a block in processing is the cause of intracellular dextran accumulation.

Together, these data indicate that blocks in active macropinocytosis and macropinosome processing occur in tandem after ATR inhibition. It is important to note that, while using 70kDa dextran allows us to follow macropinocytosis, ATRi may also be impacting on other types of endocytosis.

Macropinocytosis is required to internalise integrins at TM growth-cone like structures, allowing TM de-adhesion.

Time-lapse imaging of treated glioblastoma cells revealed a de-adhesion/retraction defect at the termini of neurite structures upon ATR inhibition, resulting in their increasing lengthening and fragility over time, leading to destabilisation and ultimately breakage. (Fig 4A; Fig S4A; SV 1, 2). This supports the observation in Fig 3D where TM length was shown to be significantly shorter after 24 hours of ATRi treatment.

The parallel observations of a de-adhesion/retraction defect caused by an inability of TMs to release from the extra cellular matrix (ECM), plus a block in macropinocytosis are intriguing, and raise the possibility of a mechanistic connection between the two phenomena.

13

Immunofluorescent staining of E2 cells treated with ATRi revealed enrichment of integrin α6 on the surface of the stalled macropinosomes (Fig. 4B). We hypothesised that macropinocytosis may be required for rapid release of neurite growth cone-like structures through integrin internalisation and hence allow active migration of glioblastoma cells. This hypothesis is supported by observed rapid adhesion/de-adhesion in the highly dynamic growth cone like structure of glioblastoma cells grown in 3D, suggestive of a requirement for bulk trafficking of integrins.

To investigate this hypothesis, we performed internalisation assays for α5, α3 and α6 integrins. Transferrin R (TrnR) is passively, as opposed to actively, internalised and was used as a negative control. The data in Fig 4C (i)- (iv) clearly indicate that internalisation of all three integrins is reduced upon treatment with ATRi, providing further evidence of a role of ATR in regulating integrin internalisation. The reduction is modest, suggesting that internalization may be occurring in a discrete location in the cell i.e., at the growth cone-like structures at the ends of neurite protrusions.

To investigate this, we over expressed GFP-labelled α5 integrin in G7 cells and used super-resolution, time-lapse microscopy to look at 70kDa dextran uptake at growth cone like structures at the ends of neurites (Fig 4D(i)). Cells were incubated in TR-dex before addition of DMSO or ATRi. In control cells we obtained clear evidence that macropinocytosis was occurring at areas of membrane retraction, and that many of the resulting macropinosomes were positive for both GFP-α5 integrin and TR-dex (confirmed by imaging at higher temporal resolution, data not shown; Fig 4D(ii), SV3; separated fluorescence panels in Fig S4B). In addition to a subset of larger macropinosomes that were largely static, we observed a population of highly mobile smaller macropinosomes consistent with observations from studies in neuronal crest cells [26]. We also observed dextran negative endosomes of a range of sizes, some of which are likely too small to be macropinocytotic in origin.

Importantly, we observed that treatment with ATRi downregulated *de novo* macropinocytosis, with all pre-existing, internalised macropinosomes becoming static (Fig 4D (iii), (iv); SV4; separated fluorescence panels in Fig S4B). This latter observation indicates defective trafficking of the structures through the cytoplasm, either to be recycled to the membrane or shuttled to the lysosomes for degradation.

These data provide strong evidence to support our hypothesis that ATR is required for effective internalisation of integrins and subsequent de-adhesion and retraction of TMs to enable effective migration *in vitro* and *in vivo*.

14

ATRi causes a reduction in actin cytoskeleton and microtubule plasticity.

Since our results indicate that ATRi inhibits cell motility, active macropinocytosis and endosomal processing, we hypothesised that ATRi may be inhibiting actin cytoskeleton dynamics, which support these processes. We examined actin cytoskeleton dynamics by treating E2 and R15 cell lines with DMSO, ATRi or ATRiB followed by high-throughput imaging after immunofluorescent staining for pMLC2, a marker of actin cytoskeleton contractility. An inhibitor of MRCK (BDP9066) was used as a positive control [5]. We observed a significant decrease in pMLC2 levels in both cell lines after treatment with both ATR inhibitors, indicating a reduction in actin cytoskeleton contractility (Fig 5A (i-iii). Total MLC2 was unchanged (Fig S5).

As we also observe a reduction in endosomal trafficking, we looked for involvement of the microtubule network in our observed phenotypes. Microtubules serve as tracts to allow trafficking of intracellular cargo, including endosomes. EB1 binds to the plus end of microtubules and can be used to track their dynamic growth [40]. GFP-EB1 was transiently expressed in G7 cells followed by treatment with either DMSO, ATRi, ATRiB or MRCKi for 16 hours. Timelapse confocal imaging was undertaken to capture EB1 dynamics (Fig 5B, SV5). Automated tracking software was used to track XYZ EB1-GFP foci position over time and measure average speed (Fig 5B (ii); SV6). Treatment with both inhibitors significantly reduced EB1 foci speed, indicating that the microtubule network is also impacted by ATRi. Although MRCK is primarily an inhibitor of actin-myosin dynamics and does not act directly on the microtubule networks, the substantial crosstalk between the two cytoskeletal components causes microtubule dysregulation following prolonged MRCKi (16hours), and therefore we used this inhibitor as a positive control. We also treated cells with the microtubule polymerization inhibitor, nocodazole, and saw rapid loss of EB1 foci, confirming the specificity of our tracking experiments (data not shown).

These data strongly indicate that ATRi inhibits cell motility, macropinocytosis and endosomal trafficking by reducing the dynamics of the actin cytoskeleton and microtubule networks. As further confirmation, we performed subconfluent migration assays following treatment with DMSO, ATRi, MRCKi or combination treatment with both inhibitors (Fig 5C). We saw no evidence of an additive or synergistic effect, suggesting that ATRi does indeed abrogate migration via downregulation of cytoskeletal activity.

15

Inhibition of ATR opposes glioblastoma cell infiltration *in vivo.*

Initial pharmacokinetic studies demonstrated tumour penetration of VX970 in an intracranial model of glioblastoma (G7) at levels sufficient to inhibit the kinase and induce phenotypic effects (Fig 6A). Importantly, drug delivery was enhanced in the tumour compared to the contralateral brain, thereby enhancing tumour specificity. We tested the ability of ATRi to inhibit glioblastoma invasion *in vivo* using the same intracranial model (G7). Tumours were allowed to develop for 10 weeks then treated with ATRi and sacrificed (Fig 6B (i)). The brains were fixed and sectioned then stained for Ki67 to label proliferating glioblastoma cells within the non-proliferative brain tissue, using a previously validated method (via correlation with Human leukocyte antigen (HLA)) for quantifying invasion [5]. Subsequent automated analysis revealed that invasion was significantly decreased in mice treated with ATRi (Fig 6B (ii)). To validate this result, we repeated the experiment using the highly infiltrative S24 cell line (Fig 6C(i)) and observed a significant decrease in the percentage of invading glioblastoma cells in the contralateral hemisphere following treatment with ATRi (Fig 6C (ii)).

Finally, the intracranial window model was employed to monitor morphology pre- and post- treatment. Mice (n=5) were treated twice with vehicle, followed by multiphoton imaging of tumour cells within the brain. The same mice were then treated twice with ATRi followed by repeat multiphoton imaging (Fig 6B (ii)). Measurement of TM length under control and treatment conditions revealed a significant decrease in length indicative of reduced invasive potential (Fig 6B (iii), (iv)).

Discussion

We present data that describe a novel, non-canonical role for ATR kinase in facilitating tumour cell motility and invasion via macropinocytic internalisation of integrins and identify ATR as a readily translatable target to achieve containment of disease dissemination in glioblastoma.

Inhibiting invasion has been shown to correlate with increased mouse survival in previous studies using different glioblastoma models [5,6]. We show with three separate *in vivo* experiments that inhibition of ATR with VX970 effectively abrogates invasion. *In vitro* we demonstrate the efficacy of two separate ATR inhibitors, as well RNAi, in inhibiting glioblastoma cell motility. Furthermore, we show that over-expression of ATR can drive increased motility, conferring on ATR an active role in regulation of cell migration.

Our novel observation linking macropinocytosis to invasion in glioblastoma opens an intriguing and exploitable therapeutic vulnerability. Macropinocytosis is involved in the bulk trafficking of integrins to

16

allow active migration and is a prominent feature in glioblastoma [27,28,41,42]. The importance of macropinocytosis in growth cone de-adhesion and neurite retraction/redirection has previously been described in neuronal cells [23,24]. TMs of glioblastoma cells share multiple properties with the neurite projection of neuronal cells, including the presence of growth cones, the ability to probe and respond to the local environment through dynamic movement, and even the ability to form functional synapses [17-19]. Glioblastoma cells protrude long TMs into the normal brain that one could postulate are sensing the new environment, before committing to invasion. In this situation, the ability to de-adhere rapidly to allow retraction or redirection in response to positive or negative environmental cues would be advantageous. Indeed, macropinocytosis has also been implicated in chemotaxic response, and nutrient sensing [20,21].

While the canonical functions of ATR in replication stress and DNA damage signalling in glioblastoma are well characterised, we demonstrate for the first time that ATR is required to mediate internalisation of integrins and subsequent trafficking of endosomes to allow active migration in glioblastoma cells [14-16]. Upon first consideration, this observation may be surprising. However, the ability of ATR to trigger cell cycle arrest and modulate kinesins and cytoskeletal dynamics provide a compelling mechanistic link [43] [44] [14]. Indeed, our study presents the novel observation that ATR modulates cytoskeletal dynamics in glioblastoma cells, beyond the previously described context of the cell cycle.

ATR inhibitors are the subject of intense interest due to their potentiation of DNA damage in combination with conventional cytotoxic agents and radiation in a range of tumour sites. In the context of neuro-oncology, the ATR/replication stress response axis is a particularly appealing target. Treatment resistance in glioblastoma is driven by a subpopulation of radioresistant glioma stem cells and ATRi has been shown to be a potent radiosensitiser *in vitro* [30]. Our novel findings suggest a dual clinical benefit to ATRi in both reducing tumour burden and containing invasion. It could be envisaged that ATRi could also be employed in an adjuvant setting to reduce malignant infiltration into vital neural structures.

In summary we present a novel role for ATR in regulating glioblastoma invasion which, in addition to furthering our understanding of the mechanisms underpinning glioblastoma invasion, has significant relevance for clinical translation. We predict that this previously unappreciated function of ATR will lead to unexpected clinical benefits from therapeutic strategies combining ATR inhibition with radiotherapy.

17

Author Contributions

Conception and design: JLB, RC, JN, AJC

Development of methodology: JLB, RC, DHH, EM, PT, LC, GS, FW

Acquisition of data (provided animals, acquired and managed patients, provided facilities, etc.): JLB, RC, K.S, SD, LD, L G, YT, WY, KM, EM, PT, CLM, AV, SJC, OR, LL

Analysis and interpretation of data (e.g., statistical analysis, biostatistics, computational analysis): JLB, RC, K.S, SD, LD, L G, YT, WY, KM, EM, PT, CLM, AV, SJC, OR, LL

Writing, review, and/or revision of the manuscript: JLB, RC, JN, AJC

18

References

1. Drumm MR, Dixit KS, Grimm S, et al. Extensive brainstem infiltration, not mass effect, is a common feature of end-stage cerebral glioblastomas. *Neuro Oncol.* 2020; 22(4):470-479.
2. Stupp R, Mason WP, van den Bent MJ, et al. Radiotherapy plus concomitant and adjuvant temozolomide for glioblastoma. *N Engl J Med.* 2005; 352(10):987-996.
3. Wegner RE, Abel S, Horne ZD, et al. National trends in radiation dose escalation for glioblastoma. *Radiat Oncol J.* 2019; 37(1):13-21.
4. Walker MD, Alexander E, Jr., Hunt WE, et al. Evaluation of BCNU and/or radiotherapy in the treatment of anaplastic gliomas. A cooperative clinical trial. *J Neurosurg.* 1978; 49(3):333-343.
5. Birch JL, Strathdee K, Gilmour L, et al. A Novel Small-Molecule Inhibitor of MRCK Prevents Radiation-Driven Invasion in Glioblastoma. *Cancer Res.* 2018; 78(22):6509-6522.
6. Edalat L, Stegen B, Klumpp L, et al. BK K+ channel blockade inhibits radiation-induced migration/brain infiltration of glioblastoma cells. *Oncotarget.* 2016; 7(12):14259-14278.
7. Kegelman TP, Wu B, Das SK, et al. Inhibition of radiation-induced glioblastoma invasion by genetic and pharmacological targeting of MDA-9/Syntenin. *Proc Natl Acad Sci U S A.* 2017; 114(2):370-375.
8. Yazinski SA, Zou L. Functions, Regulation, and Therapeutic Implications of the ATR Checkpoint Pathway. *Annu Rev Genet.* 2016; 50:155-173.
9. Carruthers RD, Ahmed SU, Ramachandran S, et al. Replication Stress Drives Constitutive Activation of the DNA Damage Response and Radioresistance in Glioblastoma Stem-like Cells. *Cancer Res.* 2018; 78(17):5060-5071.
10. Qiu Z, Oleinick NL, Zhang J. ATR/CHK1 inhibitors and cancer therapy. *Radiother Oncol.* 2018; 126(3):450-464.
11. Lecona E, Fernandez-Capetillo O. Targeting ATR in cancer. *Nat Rev Cancer.* 2018; 18(9):586-595.
12. Simon DN, Wilson KL. The nucleoskeleton as a genome-associated dynamic 'network of networks'. *Nat Rev Mol Cell Biol.* 2011; 12(11):695-708.
13. Lottersberger F, Karssemeijer RA, Dimitrova N, de Lange T. 53BP1 and the LINC Complex Promote Microtubule-Dependent DSB Mobility and DNA Repair. *Cell.* 2015; 163(4):880-893.
14. Cara L, Baitemirova M, Follis J, Larios-Sanz M, Ribes-Zamora A. The ATM- and ATR-related SCD domain is over-represented in proteins involved in nervous system development. *Sci Rep.* 2016; 6:19050.
15. Kidiyoor GR, Li Q, Bastianello G, et al. ATR is essential for preservation of cell mechanics and nuclear integrity during interstitial migration. *Nat Commun.* 2020; 11(1):4828.
16. Cheng A, Zhao T, Tse KH, et al. ATM and ATR play complementary roles in the behavior of excitatory and inhibitory vesicle populations. *Proc Natl Acad Sci U S A.* 2018; 115(2):E292-E301.
17. Jung E, Alfonso J, Osswald M, Monyer H, Wick W, Winkler F. Emerging intersections between neuroscience and glioma biology. *Nat Neurosci.* 2019; 22(12):1951-1960.
18. Osswald M, Jung E, Sahm F, et al. Brain tumour cells interconnect to a functional and resistant network. *Nature.* 2015; 528(7580):93-98.
19. Venkataramani V, Tanev DI, Strahle C, et al. Glutamatergic synaptic input to glioma cells drives brain tumour progression. *Nature.* 2019; 573(7775):532-538.
20. King JS, Kay RR. The origins and evolution of macropinocytosis. *Philos Trans R Soc Lond B Biol Sci.* 2019; 374(1765):20180158.
21. Lim JP, Gleeson PA. Macropinocytosis: an endocytic pathway for internalising large gulps. *Immunol Cell Biol.* 2011; 89(8):836-843.

19

22. Mylvaganam S, Freeman SA, Grinstein S. The cytoskeleton in phagocytosis and macropinocytosis. *Curr Biol.* 2021; 31(10):R619-R632.

23. Kabayama H, Takeuchi M, Taniguchi M, et al. Syntaxin 1B suppresses macropinocytosis and semaphorin 3A-induced growth cone collapse. *J Neurosci.* 2011; 31(20):7357-7364.

24. Kolpak AL, Jiang J, Guo D, et al. Negative guidance factor-induced macropinocytosis in the growth cone plays a critical role in repulsive axon turning. *J Neurosci.* 2009; 29(34):10488-10498.

25. Gu Z, Noss EH, Hsu VW, Brenner MB. Integrins traffic rapidly via circular dorsal ruffles and macropinocytosis during stimulated cell migration. *J Cell Biol.* 2011; 193(1):61-70.

26. Li Y, Gonzalez WG, Andreev A, et al. Macropinocytosis-mediated membrane recycling drives neural crest migration by delivering F-actin to the lamellipodium. *Proc Natl Acad Sci U S A.* 2020; 117(44):27400-27411.

27. Colin M, Delporte C, Janky R, et al. Dysregulation of Macropinocytosis Processes in Glioblastomas May Be Exploited to Increase Intracellular Anti-Cancer Drug Levels: The Example of Temozolomide. *Cancers (Basel).* 2019; 11(3).

28. Seguin L, Odouard S, Corlazzoli F, et al. Macropinocytosis requires Gal-3 in a subset of patient-derived glioblastoma stem cells. *Commun Biol.* 2021; 4(1):718.

29. Fael Al-Mayhani TM, Ball SL, Zhao JW, et al. An efficient method for derivation and propagation of glioblastoma cell lines that conserves the molecular profile of their original tumours. *J Neurosci Methods.* 2009; 176(2):192-199.

30. Ahmed SU, Carruthers R, Gilmour L, Yildirim S, Watts C, Chalmers AJ. Selective Inhibition of Parallel DNA Damage Response Pathways Optimizes Radiosensitization of Glioblastoma Stem-like Cells. *Cancer Res.* 2015; 75(20):4416-4428.

31. Rainero E, Howe JD, Caswell PT, et al. Ligand-Occupied Integrin Internalization Links Nutrient Signaling to Invasive Migration. *Cell Rep.* 2015; 10(3):398-413.

32. Winkler F, Kozin SV, Tong RT, et al. Kinetics of vascular normalization by VEGFR2 blockade governs brain tumor response to radiation: role of oxygenation, angiopoietin-1, and matrix metalloproteinases. *Cancer cell.* 2004; 6(6):553-563.

33. Li L, Wan T, Wan M, Liu B, Cheng R, Zhang R. The effect of the size of fluorescent dextran on its endocytic pathway. *Cell Biol Int.* 2015; 39(5):531-539.

34. Ravi VM, Will P, Kueckelhaus J, et al. Spatially resolved multi-omics deciphers bidirectional tumor-host interdependence in glioblastoma. *Cancer Cell.* 2022; 40(6):639-655 e613.

35. Neftel C, Laffy J, Filbin MG, et al. An Integrative Model of Cellular States, Plasticity, and Genetics for Glioblastoma. *Cell.* 2019; 178(4):835-849 e821.

36. Gomez-Roman N, Stevenson K, Gilmour L, Hamilton G, Chalmers AJ. A novel 3D human glioblastoma cell culture system for modeling drug and radiation responses. *Neuro Oncol.* 2017; 19(2):229-241.

37. Tuloup-Minguez V, Hamai A, Greffard A, Nicolas V, Codogno P, Botti J. Autophagy modulates cell migration and beta1 integrin membrane recycling. *Cell Cycle.* 2013; 12(20):3317-3328.

38. Mrschtik M, O'Prey J, Lao LY, et al. DRAM-3 modulates autophagy and promotes cell survival in the absence of glucose. *Cell Death Differ.* 2015; 22(10):1714-1726.

39. Commisso C, Flinn RJ, Bar-Sagi D. Determining the macropinocytic index of cells through a quantitative image-based assay. *Nat Protoc.* 2014; 9(1):182-192.

40. Akhmanova A, Steinmetz MO. Control of microtubule organization and dynamics: two ends in the limelight. *Nat Rev Mol Cell Biol.* 2015; 16(12):711-726.

41. Caswell PT, Vadrevu S, Norman JC. Integrins: masters and slaves of endocytic transport. *Nat Rev Mol Cell Biol.* 2009; 10(12):843-853.

42. De Franceschi N, Peuhu E, Parsons M, et al. Mutually Exclusive Roles of SHARPIN in Integrin Inactivation and NF-kappaB Signaling. *PLoS One.* 2015; 10(11):e0143423.

20

43. Fan G, Sun L, Meng L, et al. The ATM and ATR kinases regulate centrosome clustering and tumor recurrence by targeting KIFC1 phosphorylation. *Nat Commun.* 2021; 12(1):20.

44. Lamm N, Read MN, Nobis M, et al. Nuclear F-actin counteracts nuclear deformation and promotes fork repair during replication stress. *Nat Cell Biol.* 2020; 22(12):1460-1470.

21

Figure 1: A) ATR is found in both the nucleus and cytoplasm of glioblastoma cells and is associated with invasive potential. (i) R15 and G7 cells were fixed and stained with whole cell stain (red), ATR (green) and DAPI (blue). **B)** G7 cells were irradiated with 2Gy and fixed after 6 hours and stained for ATR (green), Phalloidin (yellow) and DAPI (blue) followed by high-throughput imaging and automated analysis. Data from 3 biological repeats, 2000-4000 cells imaged per condition per repeat. Bars are mean ±-SEM. Statistical analysis using student's T Test. * p<0.05, NS = not significant. **C)** ATR expression correlates with both **(i)** glioma grade and **(ii), (iii)** poorer patient survival. **D)** Increased pATR expression can be found in the invasive tumour margin versus the tumour core in patient samples. **(i)** Core and margin samples were taken from 3 different patients, stained for pATR and scored by a neuropathologist for positive cells and the fold change between core and margin plotted. **E) (i)** ATR expression is increased in primary Ox5 glioblastoma cells derived from the tumour margin compared to matched cells from the core. **(ii)** Western blot quantified from 4 independent biological repeats. Statistical analysis using student's TTest. * p<0.05. **F) (i)** Spatial transcriptomics identifies increased ATR expression in tumour margins and pseudopallisades **(ii)** ATR expression was aligned with known cell culture, spatial, single cell and bulk signatures.

Figure 2: ATR is required to drive glioblastoma cell migration *in vitro*. A(i) G7, E2 and R15 cells were plated subconfluently and treated with either DMSO or ATRi (1μM VE822) for 24 hours followed by timelapse microscopy and single cell tracking. **B)** G7 (i) and R15 (ii) cells show a dose dependent reduction in migration speed with ATR inhibition, at sub-lethal concentrations of inhibitor. Cells were incubated with DMSO/ ATRi for 24hours followed timelapse microscopy and single cell tracking or viability assay. **C) (i)** G7 cells were plated subconfluently and treated with either DMSO or ATRiB (1μM Bayer 1895344) for 24hours followed by timelapse microscopy and single cell tracking. **(ii)** G7 cells were treated with siRNAs targeting ATR or 1μM ATRi (VE822) followed by timelapse microscopy and single cell tracking. ATR knockdown was confirmed by western blot **(iii)**. D= DMSO; NT = Non-targeting siRNA. **D) (i)** ATR was over-expressed in G7 cells followed by timelapse microscopy and single cell tracking. **(ii) and (iii)** Over-expression was confirmed by western blot (n=2, error bar = std dev). **(ii)**. EV= Empty vector (pcDNA3**).** For all motility assays, data from 3 biological repeats, >30 cells tracked per repeat (grey). Two tailed, unpaired students T Test were performed on means from each biological repeat (red). For siRNA in C(ii) a one way ANOVA and Dunnett's test was performed. *p<0.05, ** p<0.01, *** p<0.001, n.s. = non-significant.

22

Figure 3: Inhibition of ATR causes a decrease in active macropinocytosis and endocytic processing. A) (i) An accumulation of large vacuoles following either treatment with ATRi was observed in all 3 cell lines, E2 shown as an example. **(ii)** Number of vacuoles per cell following ATRi or RNAi of ATR was quantified in G7 cells, statistical significance was determined using a one way ANOVA and Dunnett's test. **B)** Electron microscopy of G7 cells showed vacuoles to be single membrane bound. **C) (i)** E2 cells incubated with 70kDa Texas red dextran (Red) alongside ATRi or DMSO. White = whole cell stain, blue = DAPI. **D)** Treatment of mice with ATRi (VX970) in an intracranial window model causes an accumulation of labelled dextran *in vivo*. **(i)** Multiphoton imaging and processing was used to detect uptake of fluorescent dextran in to GFP-S24 cells in the mouse brain. **(ii)** 5 mice were treated with DMSO and Cascade blue labelled dextran followed by imaging, then treated with ATRi and Texas red labelled dextran followed by second imaging in a longitudinal experiment (one mouse received only ATRi plus CB-Dex). **(iii)** Pearson's coefficient was calculated under each treatment condition for each mouse to estimate colocalization of dextran with S24-GFP cells using Imaris colocalization tool. > 3 images per imaging session per mouse, image data plotted individually (small points) or as mean for each mouse (large points), colour coded for each mouse. **p <0.01, Students T Test. **E)** Timed experiments demonstrate ATRi inhibits both the uptake and downstream degradation of internalised dextran. **(i)** G7 cells were incubated with DMSO, ATRi or EIPA for 15 mins or 2 hours before incubation with labelled dextran. **(ii)** G7 cells were pre-incubated with dextran to allow uptake before addition of DMSO, ATRi or EIPA. Data represents 3 biological repeats, 2000-4000 cells quantified via high throughput imaging per condition per repeat. Statistical significance was determined using a one way ANOVA and Dunnett's test. * *p* < 0.05; **p <0.01, n.s = not significant.

Figure 4: Macropinocytosis is required to internalise integrins at TM growth-cone like structures, allowing TM de-adhesion, retraction and cell migration. A) Timelapse of migrating G7 cells following 24 hours of ATRi/DMSO exposure. Arrows indicate the termini of neurites. **B)** E2 cells were treated with DMSO or 1μM ATRi for 5 hours, followed by fixing and staining for WCS (white), Integrin α6 (red). **C)** G7 cells were treated with DMSO or 1μM ATRi before lysis and measurement of internalised pool of integrins. Data from 3 independent experiments. ** *p* >0.01, Mann-whitney. **D) (i)** Super resolution microscopy was used to image the growth-cone like structures at the ends of glioblastoma neurites. **(ii)** G7 cells expressing GFP-α5 integrin (green) were incubated with 70kDa Texas red dextran (red) followed by DMSO **(ii)** or VE822 **(iii)** prior to super resolution, time-lapse imaging of growth cones. Yellow = colocalization. White arrows indicate areas of membrane retraction; red arrows indicate dextran positive macropinosomes. **(iv)**

23

Speed of intracellular trafficking of endosomes was measured using automated tracking in Imaris. Data from 3 super resolution images of growth cones per condition. Statistical analysis students ttest **** *p* >0.001

Figure 5: ATRi causes a reduction in actin cytoskeleton and microtubule plasticity. A) R15 and E2 cells were incubated with DMSO, 1µM ATRiB, 1µM ATRi or 1µM MRCKi for 6 hours before staining with antibody against pMLC2 (green), whole cell stain (red) and DAPI (blue) followed by high-throughput imaging and automated analysis. Images from R15 shown as an exemplar. Data from 3 biological repeats, 2000-4000 cells imaged per condition each repeat. Bars are mean ±-SD . Statistical significance was determined using one way ANOVA and Dunnett's test ** *p* >0.01 *** *p* >0.005. **B) (i)** EB1-GFP was transiently expressed in G7 cells, incubated with DMSO, ATRi, ATRiB or MRCKi for 16 hours **(ii)**, followed super resolution timelapse imaging and 3D automated tracking of EB1-GFP foci in Imaris. EB1-GFP foci tracking data from two biological repeats (colour coded). Each point represents data from a single image (1-3 cells) with > 100 EB1-GFP foci tracked per image. * *p* < 0.05, Students T test. **C)** G7, E2 and R15 cells were plated subconfluently and treated with either DMSO, ATRi (1µM VE822), MRCKi (1 µM BDP9066) or combined treatment for 24hours followed by timelapse microscopy and single cell tracking. Statistical analysis = one-way anova; *p<0.05, ** p<0.01, *** p<0.001, **** p<0.0001.

Figure 6: Inhibition of ATR opposes glioblastoma cell infiltration *in vivo*. A)) Pharmacokinetic (PK) analysis of VX970 delivery to G7 intracranial tumours and normal brain (contralateral hemisphere). **B) (i)** Intracranial injection of G7 cells was undertaken and tumours allowed to develop for 10 weeks, followed by 2 weeks of treatment with vehicle or VX970. Percentage Ki67 positive GLIOBLASTOMA cells outside tumour bulk were calculated using automated analysis. **C) (i)** Intracranial injection of S24 cells and tumours allowed to develop for two weeks followed by 2 weeks of treatment with vehicle or VX970 and cull of animals at a timed endpoint and processed as in **B).** For both **B** and **C**, 2-4 sections/mouse was analysed and averaged, and each average/mouse plotted as a single data point. * *p* < 0.05. **D) (i)** Intracranial window mice with S24 tumours were dosed and imaged according to the schedule in **(ii)**. Tumour microtube (TM) length was measured in multiple images per mice and image data plotted individually (small points) or as mean for each mouse (large points), colour coded for each mouse. Arrows indicate TM structures. N=5, one mouse only received VX970, ** *p*>0.001. For all experiments, number of mice per cohort is indicated adjacent to the relevant data point.

24

Figure 1.

Figure 2.

26
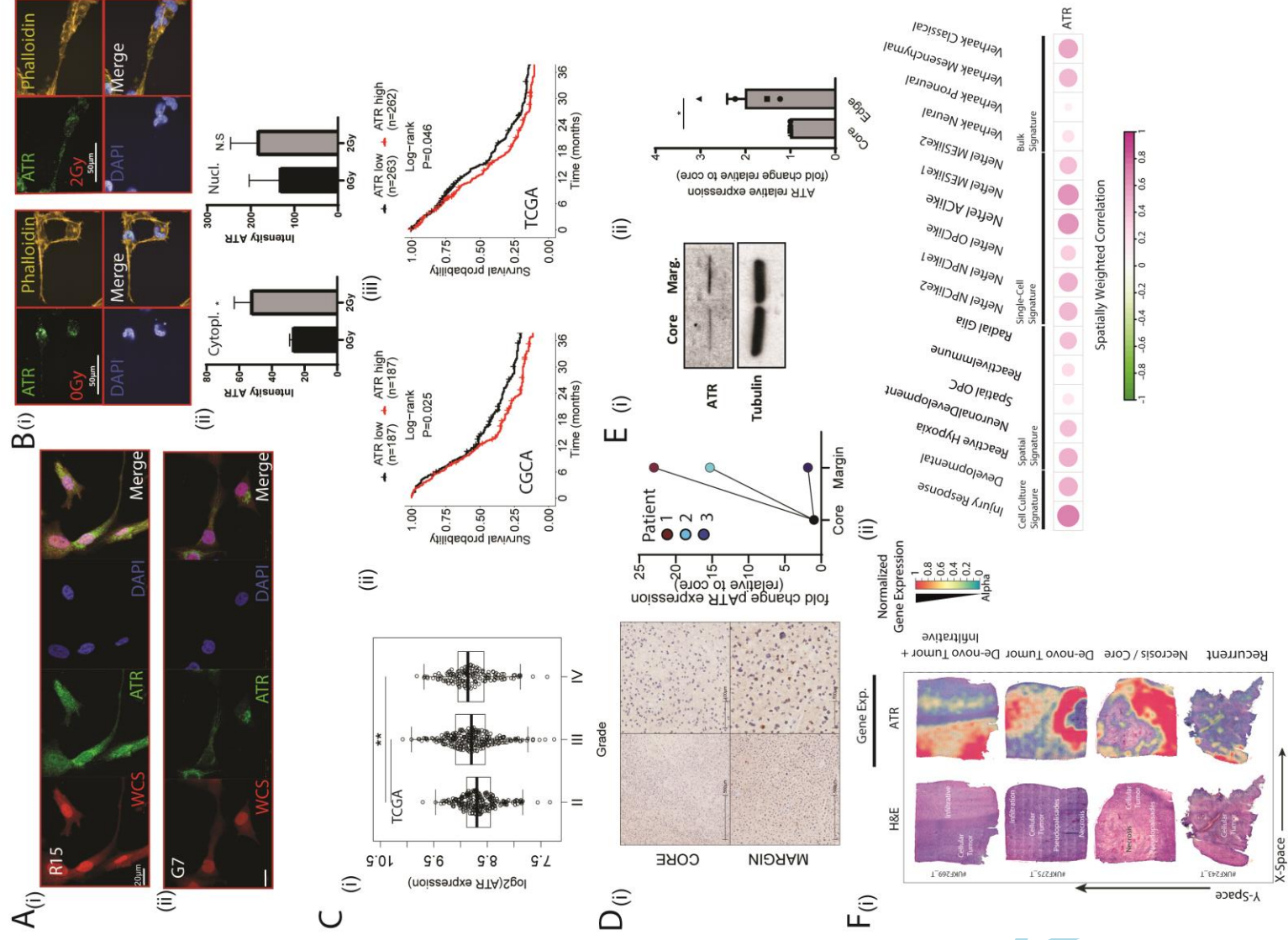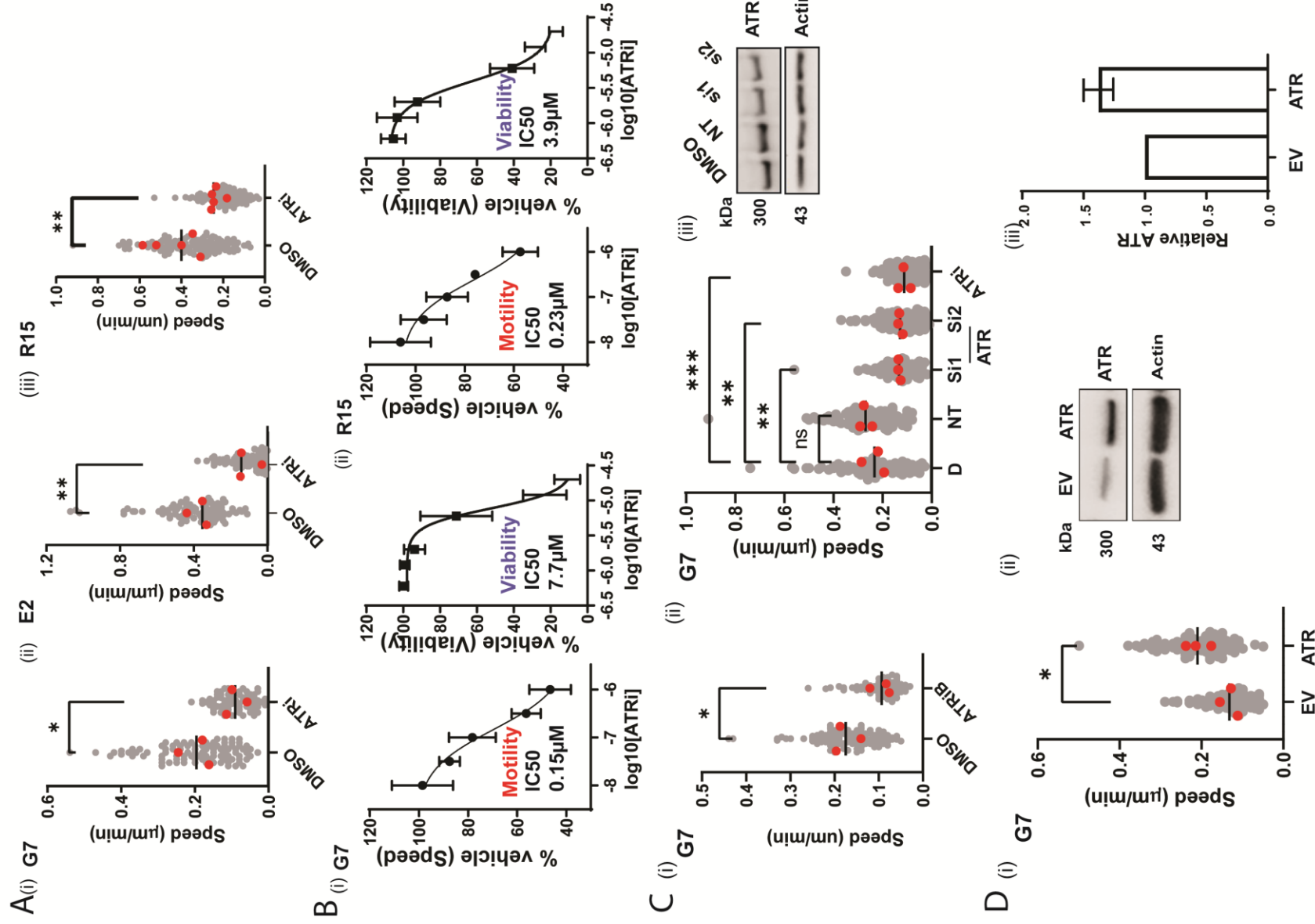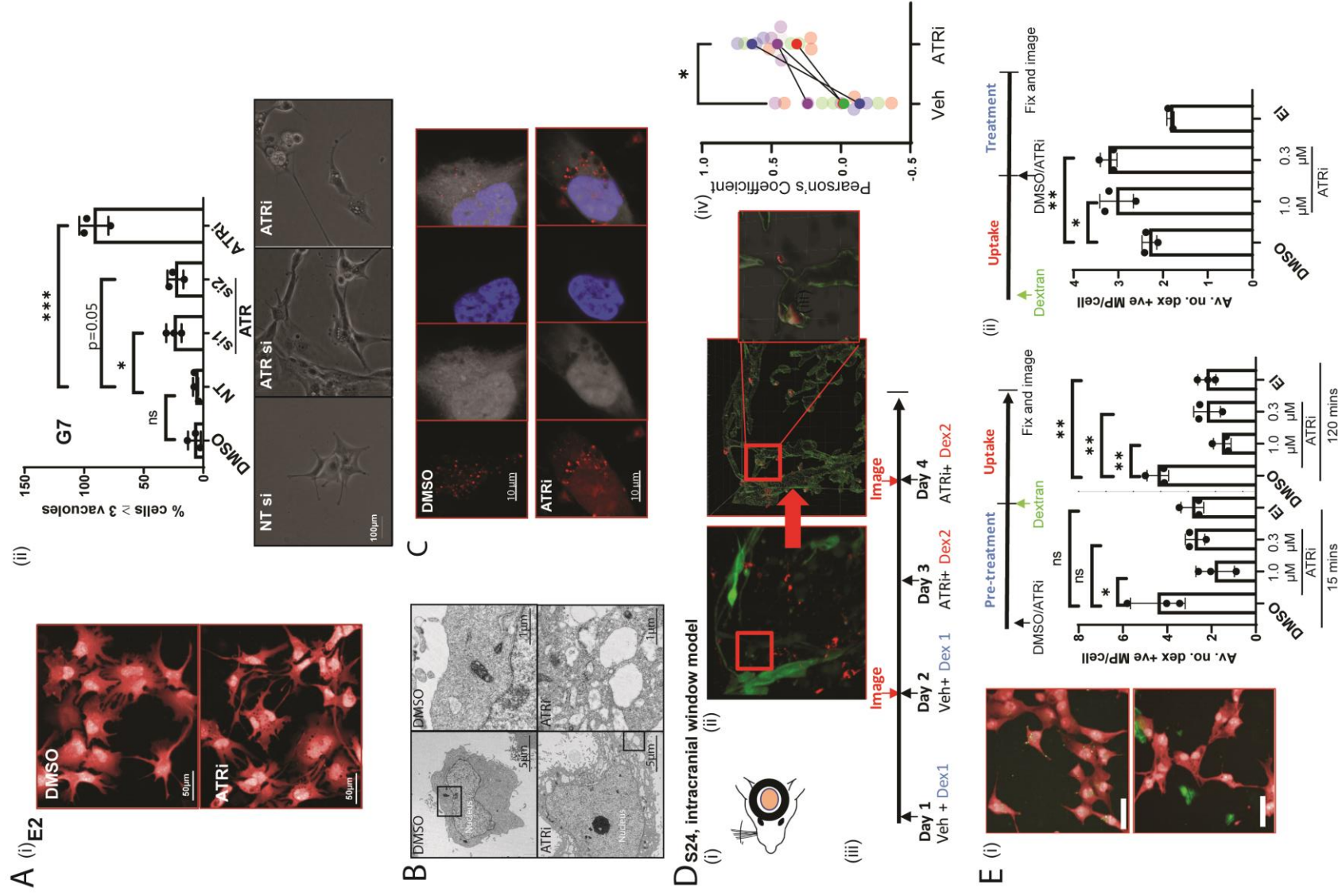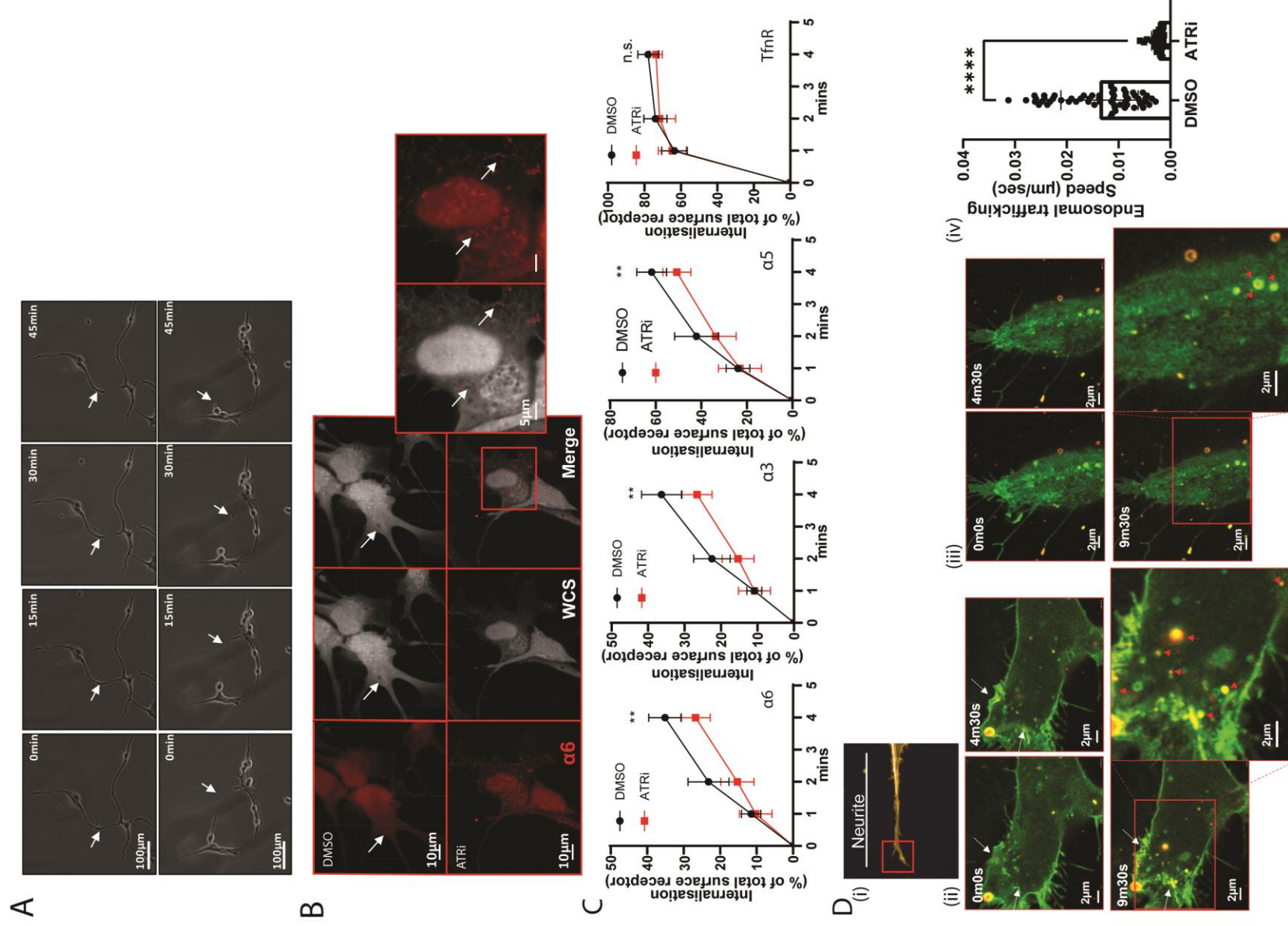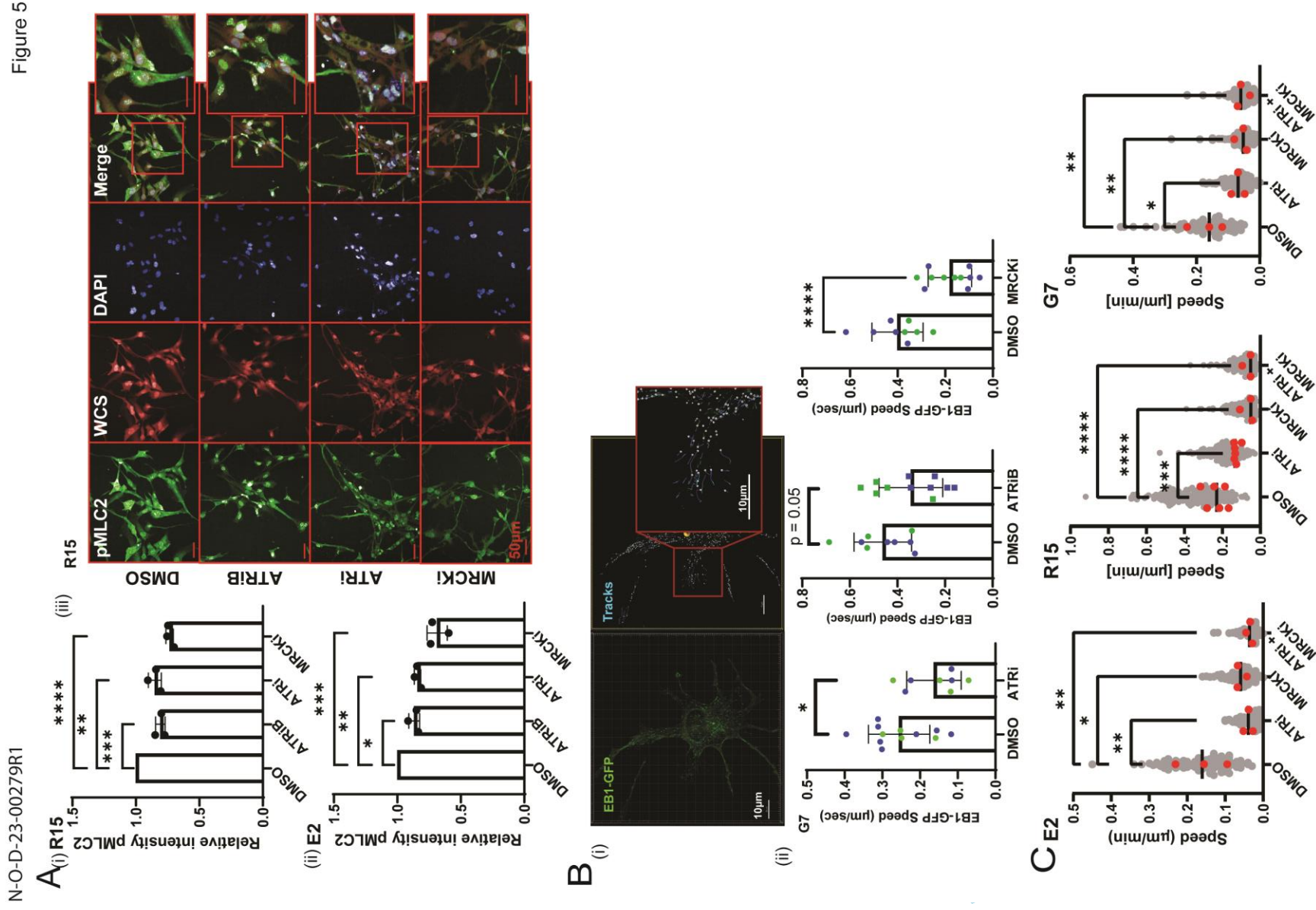
Figure 3.

N-O-D-23-00279R1

Figure 4

Figure 5

N-O-D-23-00279R1

Figure 6.